LAWRENCE
LIVERMORE
NATIONAL
LABORATORY

UCRL-JC-155353

Hot Electron Measurement and Modeling for Short-Pulse Laser Plasma Interactions

H. Chen, H. S. McLean, P. K. Patel, and S. C. Wilks

September 8, 2003

Third International Conference on Inertial Fusion Science and Applications, Monterey, California, September 7-12, 2003

HOT ELECTRON MEASUREMENT AND MODELING FOR SHORT-PULSE LASER PLASMA INTERACTIONS

H. Chen, H. S. McLean, P. K. Patel, and S. C. Wilks
Lawrence Livermore National Laboratory, Livermore, CA 94550 U.S.A.

We measured the hot electron production from short pulse laser plasma interactions using a fiber-array-based compact electron spectrometer that uses permanent magnets for electron energy dispersion and over 100 scintillating fibers coupled to a 1024 x 1024 pixel CCD as the detection system. This spectrometer has electron energy coverage from 10 keV to 60 MeV. The whole spectrometer is compact with dimensions of 8 inch × 7 inch × 4 inch. We performed systematic measurements of electron production on the ultra short pulse laser JanUSP (with pulse width less than 100 fs) at intensity range interest to Fast Ignition scheme from 10^{17} Wcm^{-2} up to 10^{19} Wcm^{-2} at Lawrence Livermore National laboratory. The electron distributions were obtained at various laser energies for different solid target materials and observation angles. We determined characteristic temperature of the escaped hot electrons at various incident laser intensity which is confirmed by theoretical simulations using the ZOHAL Particle-in-cell (PIC) code.

I. INTRODUCTION

It is long known that high-energy particles can be produced from ultra-intense short pulse laser matter interactions, which include hot electrons, ions [1-3] and positrons [4]. Hot electrons, in particular, are of interest because its characterization is critically important to the understanding of high-density plasma physics. In addition, hot electrons have many applications that making use of the temporally short, energetically broad spectrum of electrons, one prominent example is its role in the fast ignition scheme [5] for inertial confinement fusion. Two important parameters that are mostly quoted in the studies for these applications are the hot electron distribution (thereafter the effective electron temperature) and the conversion efficiency from laser energy to electrons. Although it is generally agreed that, as shown in previous studies (see review by Gibbon and Forster [2]), higher laser intensity results higher electron temperature, and at ultrahigh intensities ($I\lambda^2 > 10^{18}$ $Wcm^{-2}\mu m^2$), electrons are expected to be strongly relativistic, and their effective temperature scales with the ponderomotive potential of the laser [6], the predictions of the electron temperatures are not unambiguous due to the complicated physics processes invloved. The same is true for the experimental results. For example, electron temperatures at the ultrahigh intensities have been measured through the secondary x-ray production at various facilities [7-10], and a few hundred keV electron temperatures and up to 60% of conversion efficiencies were reported. Measurement of escaping electrons at similar intensity from solid targets [3] reported around 0.5 MeV electron temperature and 0.1% conversion efficiency, while another experiments on a gas jet target [11] found over a few MeV electron temperature and 5% of conversion efficiency.

In this paper, we report a study using a recently developed multi-channel electron spectrometer on the escaping hot electron production from solid targets irradiated by intense ultra short pulse laser at intensities $I\lambda^2 = 10^{18}$ to 10^{19} $Wcm^{-2}\mu m^2$. Electron distribution, effective temperature and laser-electron energy conversion efficiencies are presented. Measured electron temperatures have good agreement with that from the Zohar PIC simulations.

II. EXPERIMENTAL MEASUREMENT

We performed experiments on the JanUSP Ti:sapphire laser [12, 13]. It has a pulse length of 100 fs and delivers up to 10 J laser energy at 800 nm. The laser is focused with an f/2 parabola to a focus spot size of about 3.5 μm, and the laser intensity ranges from 10^{17} - 10^{20} Wcm^{-2}. The experimental setup inside the JanUSP chamber is shown in Fig 1. The target for the experiments was high purity slab (1 mm thick, 2 mm wide and 50 mm long) of plastic, aluminum, iron and gold. The laser is incident on the target at 22.5 degrees off normal. The spectrometer slit is aligned 30 degrees from the laser beam, i.e. 52.5 degrees off normal, and 23 cm away from the target. The chamber is at a vacuum of ~ 10^{-5} mbar during these experiments.

A fiber array compact electron spectrometer (FACES) was developed for the experiment. This spectrometer employs permanent magnets for electron energy dispersion and over 100 scintillating fibers coupled to a 1024x1024 pixel CCD as the detection system. The details of the spectrometer can be found in ref [14]. We made absolute calibration of the spectrometer using a pulsed electron gun. While the total number of electrons collected by the spectrometer slit to the value measured using a faraday cup, the relative electron distribution was then determined by system detection efficiency for each energy region, which include the energy absorption by the fibers at different electron energies, fiber scintillating efficiencies and transmission efficiencies and the CCD quantum efficiency.

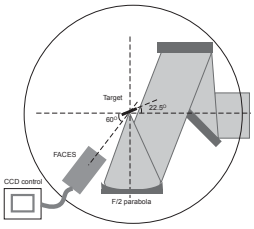

Figure 1. Diagram of the experimental setup in the JanUSP chamber

We operated the laser in the energy range from 10 mJ to 150 mJ. The magnetic strength of the spectrometer was set to either 150 Gauss or 1000 Gauss, to measure electron energies up to 1.3 MeV and 60 MeV, respectively.

III. EXPERIMENTAL RESULTS AND SIMULATIONS

Our measurements on the JanUSP laser included systematic measurements of electron production from various target materials at different detection angles and laser intensities. The experimental results are described in the following for each of these parameters.

The electron energy spectrum was measured with two separated magnet settings of the spectrometer. Figure 2 shows the measured spectra of iron target for two laser intensities. The overlap between the spectra from the two spectral settings fits very well, confirming the reliability of the measurements. As shown in the insert of Figure 2, the measured electron energy profile agrees very well with PIC simulation (as will be discussed later). The number of electrons of the simulation was normalized to the measured value for view purpose.

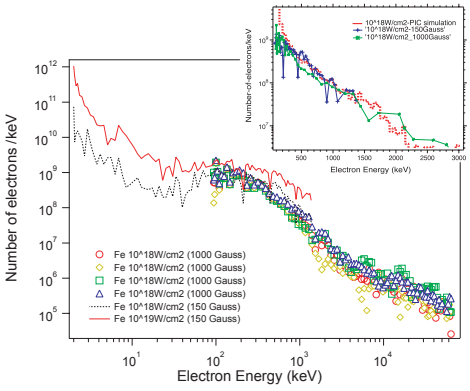

Figure 2. Electron distribution measured with two setting of the spectrometer for two laser intensities. The insert on the upper right corner shows the comparison with PIC simulation.

We have observed some differences in electron distributions as we varied the four types of laser targets CH, Al, Fe and Au. For example, there is a larger difference between the distributions between plastic

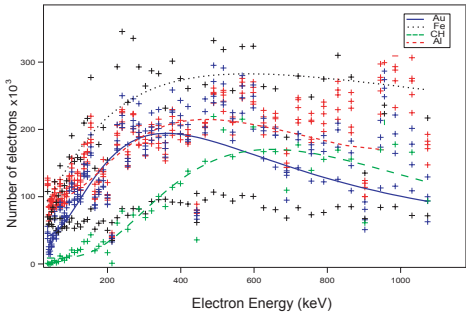

Figure 3. Electron distributions at laser intensity of 2×10^{18} Wcm^{-2} for target material of CH, Al, Fe and Au.

targets (low Z) comparing with higher Z metal targets for similar laser intensities as shown in Figure 3. This is likely due to their very different laser absorption features. However, the dependence of the electron distribution on the different metal target materials is not pronounced enough to draw conclusive remarks.

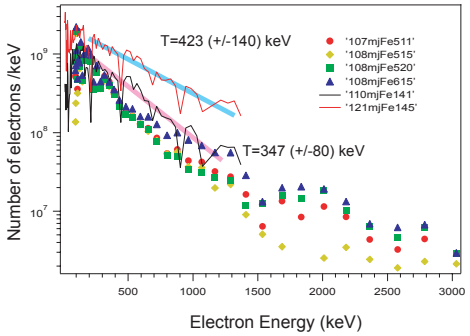

Figure 4. Effective temperatures from Bolzmann distribution fitting at two groups of laser intensities.

From fitting the electron spectrum with Boltzmann distribution, we were able to infer the effective electron temperature, as shown in Figure 4. Our measurements is sensitive to less than 10% difference in laser energy and with accuracy of about 20% ~ 30%. More electron temperature results are shown in Figure 5 for metal targets and various laser intensities. Despite the large scatter of a few data points, overall the data indicate that the lower laser intensities resulting lower electron temperature: about 200 keV and 400 keV for intensity of about 2×10^{18} Wcm^{-2} and 1×10^{19} Wcm^{-2}, respectively. It should be noted that these values have remarkable agreement with that resulted from PIC simulations, as will be discussed later.

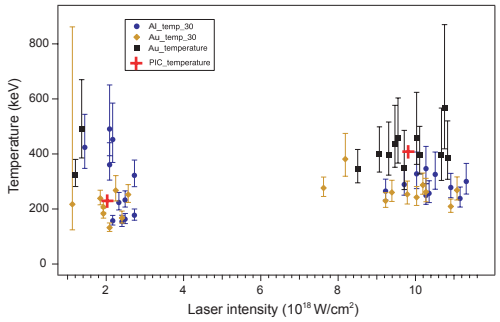

Figure 5. Electron temperatures for three laser targets at various laser intensities. The dots with error bars are from experiments, the crosses are PIC simulations.

We observed different electron distributions at different observation angle. At normal to target position, the peak of the electron energy extends higher than that from the observation at 52 degree, as shown in Figure 6. We noticed that similar observation had been made by Malka and Miquel [3].

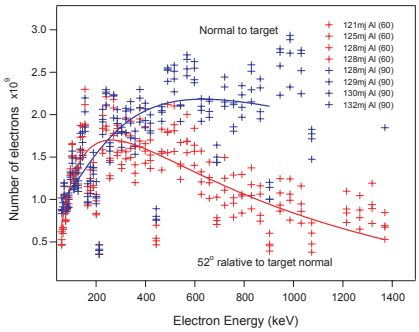

Figure 6. Electron distributions at two observation angles for Al targets at laser intensity of about 1 × 10^{19} Wcm^{-2}. Crosses are experimental data. The lines are the fits to the data.

As mentioned earlier, besides electron temperature, another important parameter to measure is the laser to electron energy conversion efficiency. Adding the energies from all the electrons we observed together, and folding in the solid angle of the detector, we can derive the total electron energy from our measurement, assuming an isotropic electron distribution (which is not precise since there is an angular dependence of electron energy distribution, although the estimated error from this assumption is less than 25%).

Figure 7 shows the ratio of the electron energy relative to the laser energy in percent. We found that between 10% and 20% of the laser energy are converted to electrons. This value is less then that obtained using secondary x-ray measurements, but higher than that from previous direct measurements.

In order to begin to understand the physics behind these measurements we have completed some 1 and 2-D fully relativistic, electromagnetic simulations using the PIC code Zohar. We begin with the 1-D cases.

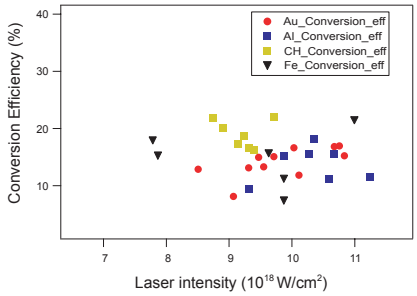

Figure 7. Conversion efficiencies form the total laser energy to hot electrons for four laser targets at different laser intensities.

Here, the laser pulse is taken to have a Gaussian temporal profile with 100 fs full-width-half-maximum. It is launched from the left (vacuum) boundary into a over dense plasma located the right-hand side with n_e/n_{cr}=70, that is approximately 26 microns long. Since there is a significant prepulse on the laser pulse, we have ramped the plasma density from 0 to 70 critical over 3 microns to model the pre-formed plasma that has been shown to exist in these interactions. The results of the electron energy distributions for the cases $2x10^{18}$ and 10^{19} W/cm^2 are plotted in Fig. 5 along with the experimental data. Reasonable agreement is found, however, it should be realized that the temperatures that the plasma achieves is somewhat dependent on the density scale length and maximum plasma density.

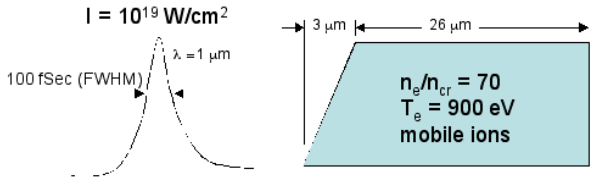

Figure 8. The laser parameters for the 1-D PIC simulations.

The laser pulse interaction in the preformed plasma just in front of the solid density target becomes even more complex when one considers 2-D effects. Consider a perfect vacuum solid interface. The laser interacts with no underdense plasma, and impinges directly onto the critical surface. The resulting B-field is shown in Fig. 9. However, even the idealized case of a perfectly Gaussian transverse laser profile propagating through a similar (but more extensive) underdense plasma is relatively complicated, as show in the B-field plot in Fig. 10. Given even this small amount of preformed plasma, filamentation can occur and the beam can

break up into just a few intense filaments, changing the entire character of the interaction. This points up the fact that a clean diagnosis of the actual amount of plasma that is present for any given experimental set-up or laser system is important if one is to understand the laser-plasma interaction in detail. Essentially, it is this that will determine the amount of preformed plasma in the interaction, and the actual amount of absorption and the electron temperatures that can be achieved. In both of these cases, the electron temperatures differ by a factor of 2 (the first case being colder) and, and thus showing the importance of knowing the preformed plasma parameters, and just how different the results can be depending on what is actually present in the experiment.

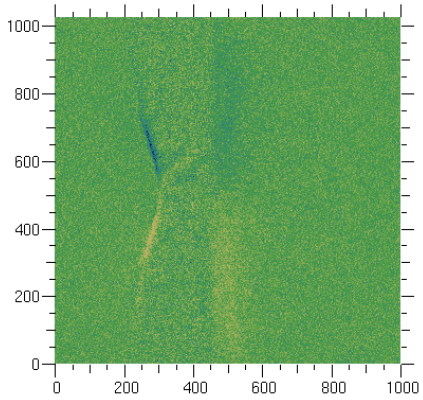

Figure 9. Resulting magnetic field of initially perfect Gaussian laser pulse propagating through 1 micron of underdense plasma before impinging on the critical surface.

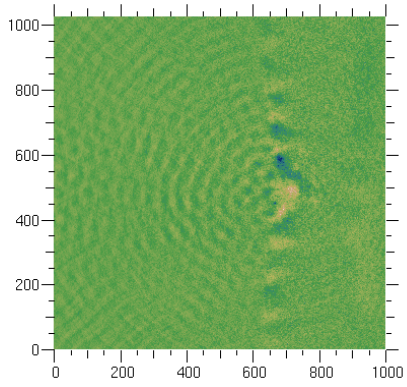

Figure 10. Resulting magnetic field of initially perfect Gaussian laser pulse propagating through 60 microns of underdense plasma before impinging on the critical surface.

IV. SUMMARY

We have performed detailed experiments on hot electron productions in Livermore short pulse facility JanUSP as well as Zohar PIC simulations. The electron energy spectrum from measurements agree with that predicted from simulation, so are the effective electron temperatures. The electron distribution as a function of observation angle was clearly observed, while its dependence of target materials is not as clear. The laser to electron energy conversion efficiency is between 10% and 20%.

ACKNOWLEDGEMENT

The work at the University of California Lawrence Livermore National Laboratory was performed under the auspice of the Department of Energy under Contract No. W-7405-Eng-48. This project was funded by the Laboratory Directed Research and Development (LDRD) Program (01-ER-100).

REFERENCES

[1] C. Darrow et al., SPIE 1860, 46 (1993)
[2] P. Gibbon and E. Forster, Plasma Phys. Control. Fusion, 38, 769 (1996)
[3] G.Malka and J.L.Miquel, Phys. Rev. Lett, 77, 75 (1996)
[4] E. P. Liang*, S. C. Wilks, and M. Tabak, Phys. Rev. Lett. 81, 4887 (1998)
[5] M. Tabak, J. Hammer, M. E. Glinsky, W. L. Kruer, S. C. Wilks, J. Woodworth, E. M. Campbell, M. D. Perry, and R. J. Mason, Phys. Plasmas 1, 1626 (1994)
[6] S. C. Wilks, W. L. Kruer, M. Tabak, and A. B. Langdon, Phys. Rev. Lett. 69, 1383 (1992).
[7] M. H. Key et al., Phys. Plasmas 5, 1966 (1998).
[8] K. B. Wharton, S. P. Hatchett, S. C. Wilks, M. H. Key, J. D. Moody, V. Yanovsky, A. A. Offenberger, B. A. Hammel, M. D. Perry and C. Joshi, Phys. Rev. Lett. 81, 822 (1998)
[9] K. Yasuike, M. H. Key, S. P. Hatchett, R. A. Snavely, and K. B. Wharton, Rev. Sci. Instruments, **72**, 1236, 2001
[10] G. Pretzler, Th. Schlegel, E. Fill, and D. Eder, Phys. Rev. E, 62, 5618 (2000)
[11] C. Gahn, G. D. Tsakiris, A. Pukhov, J. Meyer-ter-Vehn1, G. Pretzler, P. Thirolf, D. Habs, and K. J. Witte, Phys. Rev. Lett, 83, 4772 (1999)
[12] J. D. Bonlie, F. Patterson, D. Price, B. White and P. Springer Appl. Phys. B [Suppl.], 70, S155 (2000)
[13] F. Patterson, J. Bonlie, D. Price, B. White, P. Springer, Ultrafast Optics 99 Conference, Ascona, Switzerland, July 11-17, (1999).
[14] H. Chen, P. K. Patel, D. F.Price, B. K. Young, P. T. Springer, R. Berry, R. Booth, C. Bruns, and D. Nelson, Review Scientific Instruments, **74**, 1551, 2003